


12-2018

Effect of Continuity Plate Eccentricity on the Performance of Welded Beam-to-Column Connections

Jason Thomas Norwood
University of Arkansas, Fayetteville

Follow this and additional works at: <https://scholarworks.uark.edu/etd>

 Part of the [Civil Engineering Commons](#), and the [Structural Engineering Commons](#)

Recommended Citation

Norwood, Jason Thomas, "Effect of Continuity Plate Eccentricity on the Performance of Welded Beam-to-Column Connections" (2018). *Theses and Dissertations*. 2991.
<https://scholarworks.uark.edu/etd/2991>

This Thesis is brought to you for free and open access by ScholarWorks@UARK. It has been accepted for inclusion in Theses and Dissertations by an authorized administrator of ScholarWorks@UARK. For more information, please contact scholar@uark.edu, ccmiddle@uark.edu.

Effect of Continuity Plate Eccentricity on the Performance of
Welded Beam-to-Column Connections

A thesis submitted in partial fulfillment
of the requirements for the degree of
Master of Science in Civil Engineering

by

Jason Norwood
University of Arkansas
Bachelor of Science in Civil Engineering, 2017

December 2018
University of Arkansas

This thesis is approved for recommendation to the Graduate Council.

Gary S. Prinz, Ph.D.
Thesis Director

W. Micah Hale, Ph.D.
Committee Member

Cameron Murray, Ph.D.
Committee Member

Abstract

Beam-to-column connections in structural steel buildings may have varying degrees of rotational restraint and varying degrees of moment transfer. In fully restrained moment connections, shear is typically transferred through the beam web, while the moment is mostly transferred through the beam flanges which create tension/compression force couples. Column sections that are incapable of resisting these flange forces are often retrofitted with continuity plates within the connection region to improve capacity. In cases of unequal beam depths on either side of the column, an eccentricity between the framed-in beam flange and continuity plate may be required; however, limited research exists to provide guidance on an acceptable level of eccentricity. This thesis describes a parametric finite element investigation into the performance of beam-to-column moment connections having unequal beam depths and eccentric continuity plate detailing. A total of 12 detailed finite element analyses considering two column sections (W14x132 and W21x147 sections) and six levels of connection eccentricity (ranging from 0 to 6 in.) were considered. Modeling techniques considered for the parametric investigation were validated against experiments performed from the literature. Increasing the level of eccentricity between the beam flange and continuity plate resulted in decreased continuity plate participation; however, unlike current code recommendations, noticeable participation (up to 10% additional flange capacity for a W14x132 column) was observed for eccentricities up to 4 in. A new design equation for determining beam-to-column connection capacities for configurations having eccentricities is proposed.

Table of Contents

| | | |
|--------|---|----|
| 1. | Introduction..... | 1 |
| 2. | Parametric Investigation into Eccentricity Effects | 4 |
| 2.1. | Connection Configurations and Geometry | 5 |
| 2.2. | Proposed Modeling Techniques..... | 8 |
| 2.2.1. | General Overview | 8 |
| 2.2.2. | Element Type, Loading, Materials, and Boundary Conditions | 9 |
| 3. | Validation of Modeling Techniques | 12 |
| 4. | Results and Discussion | 14 |
| 4.1. | Comparison of Validation Models and Experimental Results in Graham et al. [5] | 14 |
| 4.2. | General Observations from the Parametric Simulations..... | 17 |
| 4.3. | Effect of Eccentricity on Continuity Plate Strength Contribution | 19 |
| 4.4. | Effect of Width- Thickness Ratio on Continuity Plate Participation..... | 24 |
| 4.5. | Design Recommendations | 26 |
| 5. | Conclusions..... | 28 |
| 6. | References..... | 29 |
| | Appendix..... | 31 |
| A1. | Connection Design..... | 31 |
| A2. | Calculations for Column Flange and Continuity Plate Connection Force Capacity Added | 36 |
| A3. | Selected Hysteresis Graphs..... | 37 |
| A4. | Proposed Design Approach..... | 40 |

List of Tables

| | |
|--|----|
| Table 1. Description of two-way connections modeled..... | 6 |
| Table 2. Beam-Column Connection Configurations Design Summary..... | 7 |
| Table 3. Stress-strain input values for finite element modeling | 13 |
| Table 4. Comparison of results from Graham et al. [5] with finite element results at 10% scaled imperfections..... | 16 |
| Table 5. Flange forces at FLY and FLB limit state for W14x132 column section..... | 24 |

List of Figures

| | |
|--|----|
| Figure 1. (a) Typical force transfer in beam-to-column moment connection and (b) beam flange force eccentricity due to unequal beam depths | 1 |
| Figure 2. Column limit state failure modes for: (a) flange local bending, (b) web local yielding, (c) web local crippling, and (d) web compression buckling | 2 |
| Figure 3. General configuration of the [5] eccentric stiffener tests | 3 |
| Figure 4. (a) and (b) show two moment connection configurations featuring eccentricity and (c) shows a possible alternative to eccentric continuity plates having partial depth stiffeners | 4 |
| Figure 5. Basic configuration of the connections to be modeled..... | 5 |
| Figure 6. Allowable deformation of W-shape cross section, per ASTM A6..... | 8 |
| Figure 7. General building frame (left) and the geometry of the two-way moment configuration used for this research (right) | 8 |
| Figure 8. Lateral load concentrated flange forces (top) and gravity load concentrated flange forces (bottom)..... | 10 |
| Figure 9. Mesh sizes considered in the parametric study | 11 |
| Figure 10. Boundary conditions for the two-way moment connection models | 12 |
| Figure 11. Boundary conditions and degrees of freedom for the modeling technique validation tests | 13 |
| Figure 12. Frequency analysis on a column stub with continuity plate. Mode shape scale factor of 5 times for visual representation. | 14 |
| Figure 13. W14x61 column stub with 0 in. eccentricity showing the effects of scaled imperfections..... | 15 |
| Figure 14. Comparison of the (a) results of [5] to the (b) finite element results | 16 |
| Figure 15. Progression of PEEQ on column flange at location of beam flanges for the 1.645 eccentric connection (a) 1st cycle, 0.02 rad. (b) 2nd cycle, 0.02 rad. (c) 1st cycle, 0.03 rad. | 17 |
| Figure 16. Determining column flange yield increment using Von Mises stress (a) Increment 526 (b) Increment 527 (0.03 rad.)..... | 18 |

| | |
|---|----|
| Figure 17. Standard deviation plots for FLY limit state (a)W14x132 (b)W21x147 | 19 |
| Figure 18. Column flange connection force capacity added with respect to eccentricity for (a) W14x132 FLY (b) W21x147 FLY (c) W14x132 FLB (d) W21x147 FLB | 21 |
| Figure 19. Stresses on W14x132 column flange at 2nd cycle, 0.04 rad. as eccentricity increases | 21 |
| Figure 20. Impact of selection of criteria for FLB limit state on the column flange connection force capacity added | 23 |
| Figure 21. Impact of width-to-thickness ratios of columns on effectiveness of eccentric continuity plates for (a) FLY limit state and (b) FLB limit state..... | 25 |
| Figure 22. Connection force added by continuity plates for FLB limit state | 27 |
| Figure 23. Hysteresis graphs for W14x132 configurations for various eccentricities (a) 0 in. (b) 1.645 in. (c) 4.125in. (d) 5.83 in. | 39 |

1. Introduction

Beam-to-column connections in structural steel buildings can provide varying degrees of rotational restraint and therefore varying degrees of moment transfer to the connecting steel columns. Steel beam-to-column connections range from simple connections (allowing full, unrestrained, rotation with negligible moment transfer) to fully restrained moment connections (having negligible rotation and full beam-to-column moment transfer). Partially restrained moment connections also exist, and fall somewhere in-between the simple and fully-restrained conditions [1].

In fully restrained moment connections, shear force is typically transferred through the beam web, while moment is mostly transferred through the beam flanges in a tension-compression force couple, as shown in Figure 1(a) [2]. Depending on building geometry and loading, adjacent beams (beams on either side of the column) may be subjected to differing demands that require designers to select different beam sizes. Unequal beam depths, which are sometimes unavoidable, can lead to an eccentricity (e) between the beam bottom flange forces, resulting in larger column demands (see Figure 1(b)). This thesis focuses on understanding the behavior of fully restrained beam-to-column moment connections having unequal beam depths.

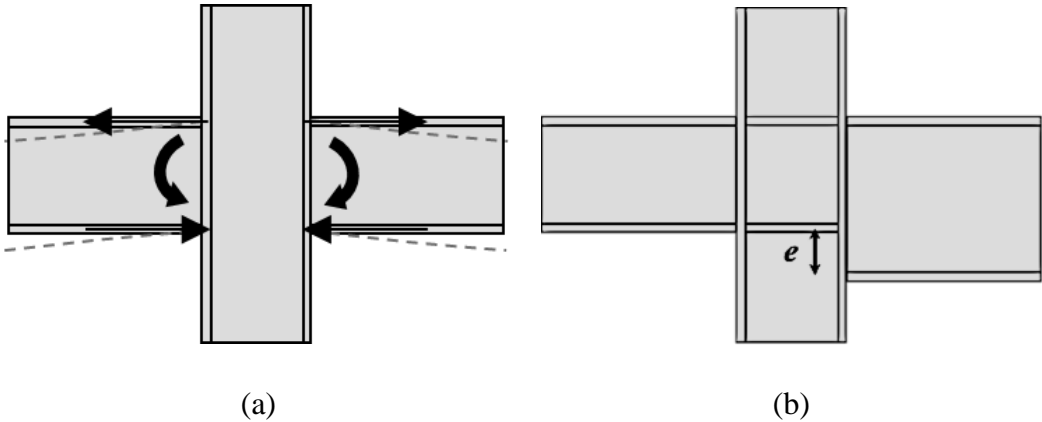


Figure 1. (a) Typical force transfer in beam-to-column moment connection and (b) beam flange force eccentricity due to unequal beam depths

Column sections incapable of transferring beam demands are often retrofitted with continuity plates within the connection region to improve capacity (see Figure 1(b)). Several column limit states exist to determine the need for continuity plates, including: 1) flange local bending, 2) web local yielding, 3) web local crippling, and 4) web compression buckling as shown in Figure 2. Continuity plates increase the strength and stiffness of column sections by transferring forces from the beam flange into the column flange and improving the transfer of force into the column web [3, 4]. Additionally, the American Institute of Steel Construction (AISC) Seismic Provisions [4] states that continuity plates improve connection performance by “...[minimizing] stress concentrations that can occur between the beam flange and the column due to non-uniform stiffness of the column flange”. There is limited research for connections having eccentricity between the framed-in beam bottom flange and continuity plate.

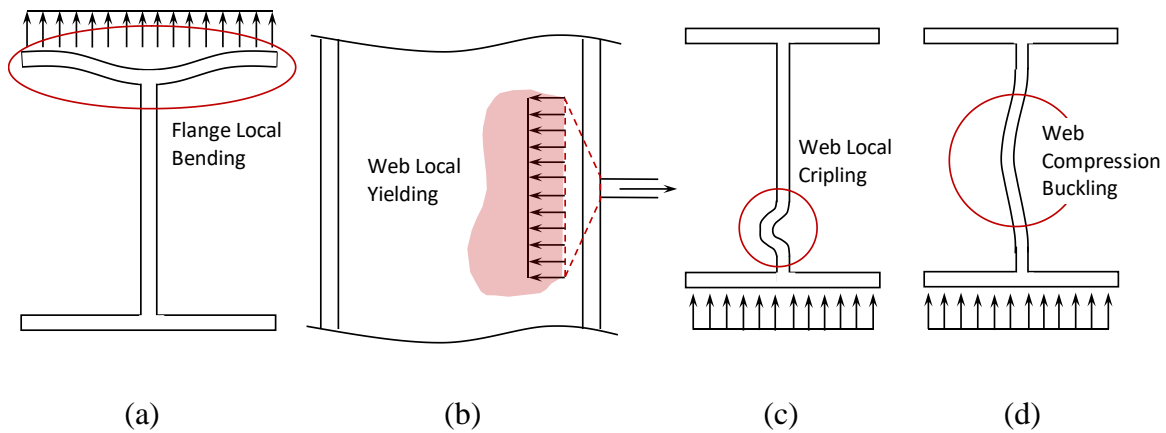


Figure 2. Column limit state failure modes for: (a) flange local bending, (b) web local yielding, (c) web local crippling, and (d) web compression buckling

Early experimental research by Graham et al. [5] investigated the effects of an eccentricity between the continuity plate and beam flange; however, the tests merely simulated the connection condition using column stubs and steel bars for beam flanges (see Figure 3). In [5], the experiments featured continuity plates having various eccentricity levels with respect to the applied loads (0, 2,

4, and 6 inches of eccentricity) and were compared to an unstiffened wide-flange control specimen containing no continuity plates. It was found that continuity plates with 2 in. eccentricity experienced a 35% reduction in strength compared to the specimen with in-line continuity plates having no eccentricity. Stub specimens having continuity plate eccentricities of 4 in. or greater experienced strength reductions greater than 80%. Based on these limited experiments, [3] limits the continuity plate contributions at an eccentricity of 2 inches with a 35% reduction in strength.

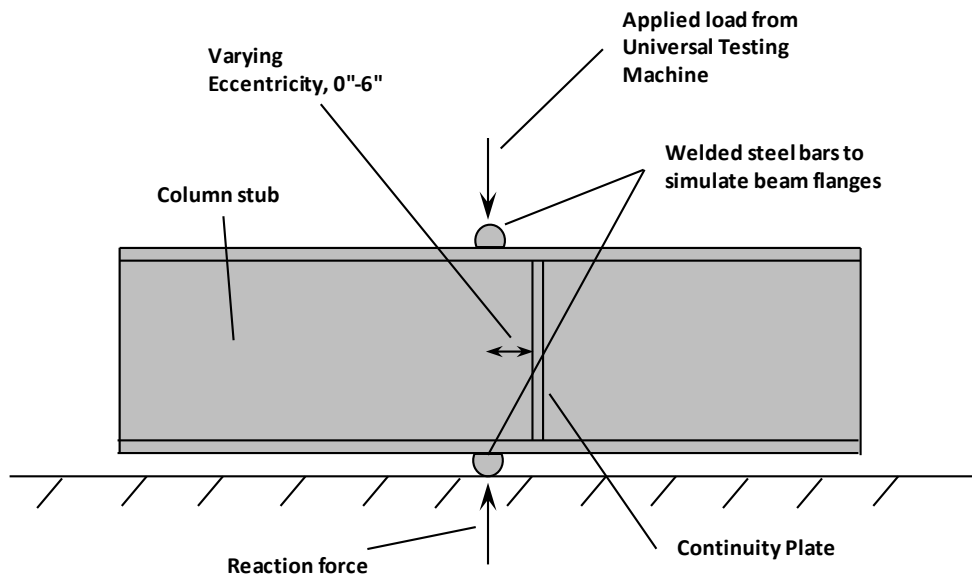


Figure 3. General configuration of the [5] eccentric stiffener tests

Eccentric stiffeners occurring in design are typically resolved as shown in Figure 4(a) and Figure 4(b); with the configuration in Figure 4(b) being used when moment connections frame into the column weak-axis. Figure 4(c) shows an additional connection detail wherein partial depth continuity plates are used when an eccentricity exceeds the 2 in. limit imposed by the specifications. Developing alternative guidelines for connection strength at larger connection eccentricities may help improve design economy for such situations.

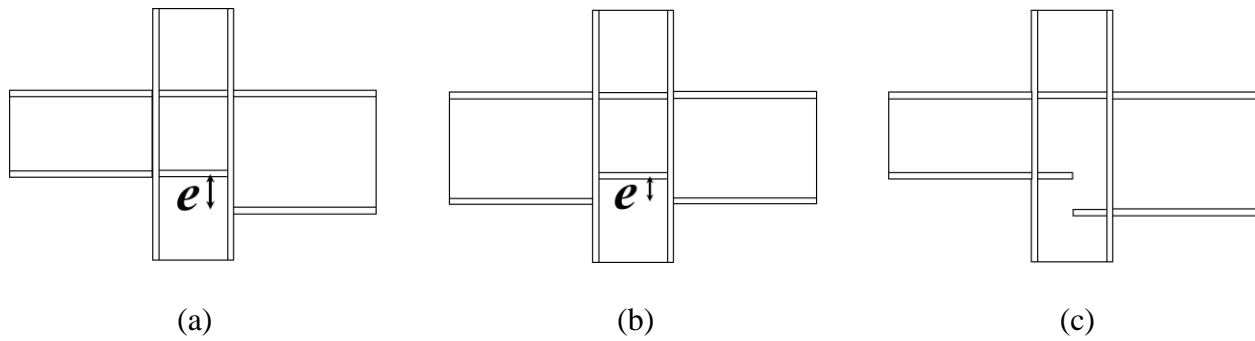


Figure 4. (a) and (b) show two moment connection configurations featuring eccentricity and (c) shows a possible alternative to eccentric continuity plates having partial depth stiffeners

This thesis describes an analytical investigation into the performance of beam-to-column moment connections having unequal beam depths and eccentric continuity plates similar to those shown in Figure 4(a). The research objective is to provide further design guidance on the level of acceptable eccentricity for both non-seismic and seismic continuity plate design requirements. In this study, a parametric analysis using advanced finite element simulations validated from experimental testing is used to estimate connection capacities in column sections having varied levels of continuity plate eccentricity. The thesis begins by describing the parametric study, including the considered connection configurations, and modeling techniques. Following, a validation study is described and results from the validation analyses and parametric investigation are presented. Next, conclusions with design recommendations are provided.

2. Parametric Investigation into Eccentricity Effects

An analytical parametric investigation was considered to investigate the effects of continuity plate eccentricity on beam-column connection performance. Two-way moment connections were considered as they can create eccentric column flange connections similar to those shown previously in Figure 4(a). Additionally, since continuity plates are primarily required in moment frame connections transferring large moments, all configurations considered herein

were designed and simulated as welded-unreinforced-flange-welded-web (WUF-W) connections in accordance with [1, 4, 6]. Figure 5 shows the basic configuration of the connections considered in the parametric investigation.

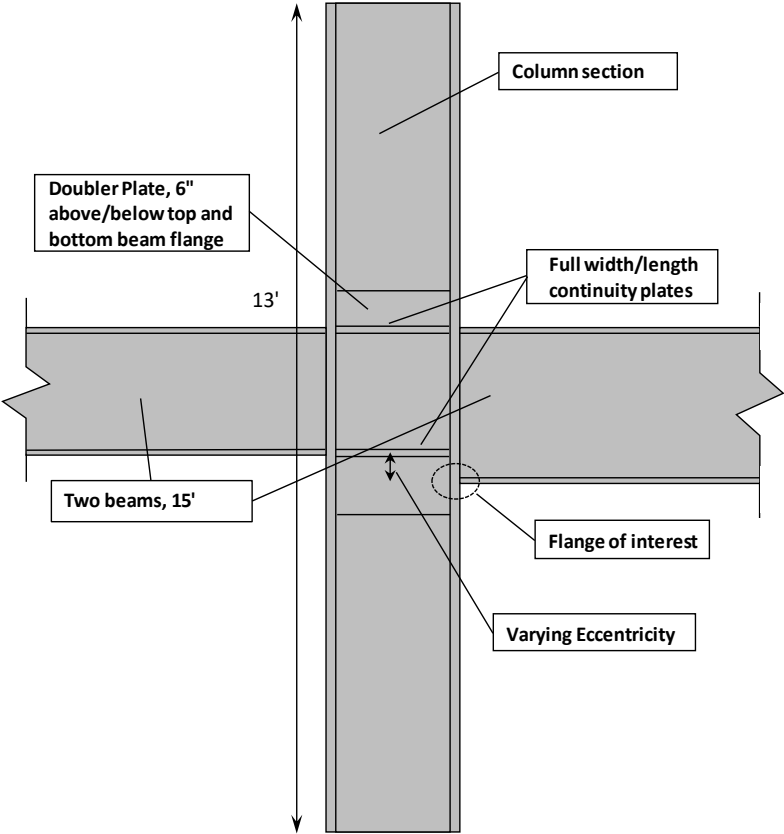


Figure 5. Basic configuration of the connections to be modeled

2.1. Connection Configurations and Geometry

A total of 12 beam-column configurations were considered in this study, representing two column sections (W14x and W21x sections), and 6 levels of beam-flange eccentricity. All configurations were designed to meet WUF-W design criteria, including: slenderness, strong column/weak beam proportioning, and doubler plate and continuity plate requirements. Each connection configuration was designed to meet general prequalification requirements for WUF-W

connection types, including a maximum beam depth of 36 in., a maximum beam flange thickness of 1 in., and a maximum beam weight of 150 lb/ft [6].

Both the W14x132 and W21x147 columns were modeled with the same beams attached, with the beams being selected so as to vary the connection eccentricity. The beams were selected to remain relatively close in weight, flange thickness, and nominal flange capacity. A description of each connection configuration is provided in Table 1.

Table 1. Description of two-way connections modeled

| Column | Beam 1 | Beam 2 | Eccentricity (in) | Column | Beam 1 | Beam 2 | Eccentricity (in) |
|---------|---------|--------|-------------------|---------|---------|--------|-------------------|
| W14x132 | W12x96 | W12x96 | 0.000 | W21x147 | W12x96 | W12x96 | 0.000 |
| W14x132 | W16x100 | W16x77 | 0.275 | W21x147 | W16x100 | W16x77 | 0.275 |
| W14x132 | W14x82 | W12x96 | 1.645 | W21x147 | W14x82 | W12x96 | 1.645 |
| W14x132 | W18x106 | W16x77 | 2.020 | W21x147 | W18x106 | W16x77 | 2.020 |
| W14x132 | W16x89 | W12x96 | 4.125 | W21x147 | W16x89 | W12x96 | 4.125 |
| W14x132 | W18x86 | W12x96 | 5.830 | W21x147 | W18x86 | W12x96 | 5.830 |

All configurations in Table 1 were selected such that column continuity plates were required to transfer the resulting beam maximum probable moment. In the configuration designs, the beam maximum probable moment (M_{pr}) was resolved into a concentrated flange force couple using Equation 1. In Equation 1, the 0.85 factor accounts for the beam web participation in moment transfer, while d_m is the moment arm between the beam flanges [4].

$$P_u = \frac{0.85 * M_{pr}}{d_m} \quad \text{Eqn-1}$$

This concentrated flange force, P_u , equals the required column strength (R_u) and must be compared to the available strengths (ϕR_n) determined from various column limit states. The limit states applicable to the connection being tested include flange local bending (FLB), web local yielding (WLY), web local crippling (WLC), web compression buckling (WCB), and web panel zone shear (PZ) [1]; however, a study by [7] found that FLB and WLY commonly control. Table 2 presents the different connection configurations considered, along with various capacity-to-demand ratios for the unstiffened configurations. Note in Table 2 that the various ratios are less

than 1, indicating that the limit state has been exceeded and that continuity plates are required to prevent FLB. Also in Table 2, the FLB and WLY limit states are fairly close to each other while the PZ limit state significantly controls. When PZ limits govern, doubler plates are required per [1] to provide sufficient strength and stiffness to the column web, which increases resistance to the WLY limit state. The required web doubler plates force flange local bending of the column flange to govern for all configurations in Table 1 (creating a consistent limit state for later performance comparison). Appendix A1 provides the calculations associated with the connection designs provided in Table 2.

Table 2. Beam-Column Connection Configurations Design Summary

| Column | Beam 1 | Eccentricity (in) | $\Phi R_n/R_u$ FLB | $\Phi R_n/R_u$ WLY | $\Phi R_w/R_u$ PZ |
|---------|---------|-------------------|-----------------------|-----------------------|----------------------|
| W14x132 | W12x96 | 0.000 | 0.45 | 0.44 | 0.24 |
| W14x132 | W16x100 | 0.275 | 0.45 | 0.44 | 0.27 |
| W14x132 | W14x82 | 1.645 | 0.54 | 0.52 | 0.27 |
| W14x132 | W18x106 | 2.020 | 0.48 | 0.47 | 0.28 |
| W14x132 | W16x89 | 4.125 | 0.51 | 0.49 | 0.26 |
| W14x132 | W18x86 | 5.830 | 0.53 | 0.51 | 0.27 |
| W21x147 | W12x96 | 0.000 | 0.56 | 0.49 | 0.37 |
| W21x147 | W16x100 | 0.275 | 0.56 | 0.50 | 0.41 |
| W21x147 | W14x82 | 1.645 | 0.67 | 0.59 | 0.39 |
| W21x147 | W18x106 | 2.020 | 0.60 | 0.54 | 0.42 |
| W21x147 | W16x89 | 4.125 | 0.63 | 0.56 | 0.38 |
| W21x147 | W18x86 | 5.830 | 0.66 | 0.57 | 0.38 |

It is important to note, that the FLB limit state is somewhat arbitrarily defined in the specifications as it is based on anecdotal effects of column flange deformations. Early research by [5] featured an equation developed for the FLB limit state, which was based on yield line analysis. This limit state was initially used as an indicator of weld fracture; however, research in [8] found that the limit state is generally conservative, and recommended a new limit for FLB based on a $\frac{1}{4}$ in. column flange deformation. The $\frac{1}{4}$ in. flange deformation comes from research in [9], which allowed the maximum depth at any cross sections over the theoretical depth for a wide-flange section to be $\frac{1}{4}$ in, as shown in Figure 6.

For this parametric study conducted herein, the allowable deformation for an individual flange was determined to be $\frac{1}{8}$ in. for the FLB limit state. While this does not strictly adhere to limits proposed in [9], it follows the intent as each flange could separate $\frac{1}{8}$ in. in opposite directions and reach the $\frac{1}{4}$ in. allowable deformation limit set forth in [9] (see Figure 6). This chosen approach is consistent with other research by [10] in a study furthering the work of [7] and [8] using cyclic loaded cruciform specimens subject to reverse curvature deformations, similar to the two-way moment configurations in this research.

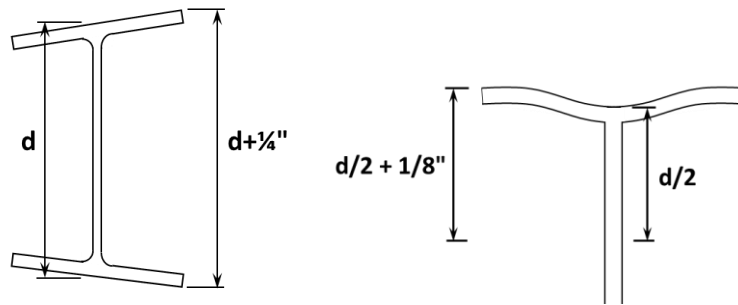


Figure 6. Allowable deformation of W-shape cross section, per ASTM A6 [9]

2.2. Proposed Modeling Techniques

2.2.1. General Overview

All two-way moment configuration simulations considered a half-column above and below the connection and a half-bay beam width on either side of the connection similar to other moment frame testing in [11-16]. Figure 7 shows the two-way moment configuration geometry considered.

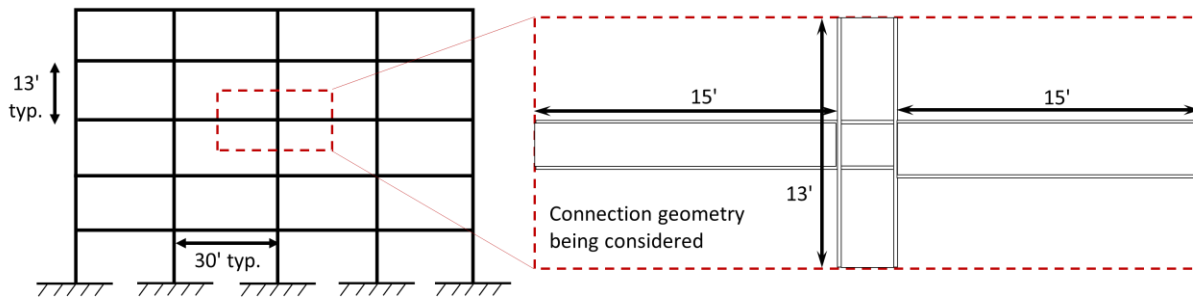


Figure 7. General building frame (left) and the geometry of the two-way moment configuration used for this research (right)

All analyses were performed using the commercial finite element program ABAQUS [17]. Specific details on the simulation element type, loading, materials and boundary conditions are presented in the following sections; however, it should be noted that weld properties and weld geometry profiles were not considered in the analyses. In a study by [8] investigating the FLB and WLY limit states, it was found that even with significant column flange deformation, none of the welds fractured in pull-plate or cruciform tests, as long as the welds met detailing requirements outlined in the specifications [1, 4, 6].

2.2.2. Element Type, Loading, Materials, and Boundary Conditions

Shell elements were used to model all geometry in the parametric study. Shell elements were chosen to allow determination of local stress and strain gradients, as well as local buckling and local element deformation (such as flange local bending). Four-node linear shell elements with reduced integration (S4R in ABAQUS) were used. Studies, including [16], have successfully used shell element geometries to capture special moment frame behavior during cyclic loading.

All connection configuration in the parametric investigation were cyclically loaded based on beam-column connection rotation histories provided in [4]. This lateral loading caused the beams to bend in reverse curvature and provide equal and opposite connection rotations as shown in Figure 8.

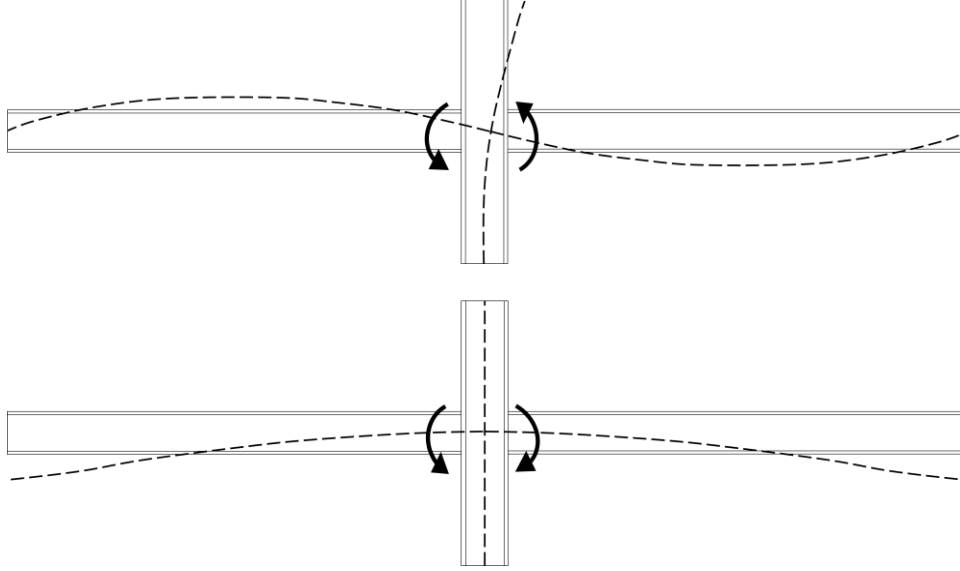


Figure 8. Lateral load concentrated flange forces (top) and gravity load concentrated flange forces (bottom)

A cyclic nonlinear kinematic material hardening model based on the plastic strain behavior of A572 Gr. 50 steel was used in this study. A572 Gr 50 is similar to A992 steel commonly used for rolled wide-flange shapes [18]. Cyclic testing of A572 Gr 50 steel was used to calibrate the material model, as the cyclic plastic strain behavior has been documented in great detail by [19]. Because large plastic strains were anticipated in the parametric simulations, material calibrations using the hardening model presented in Equation 2 were weighted toward the larger strain hysteresis curves from the material testing in [10]. Equation 2 presents the plastic material model used for the analyses, where C and γ represent kinematic hardening parameters chosen to be 406.18 and 37.175, respectively [19]. Because the number of back-stresses was 1, α_1 was set to equal zero [19].

$$\alpha = \frac{C}{\gamma} \left(1 - e^{-\gamma \varepsilon^{pl}} \right) + \alpha_1 e^{-\gamma \varepsilon^{pl}} \quad \text{Eqn-2}$$

A quad-dominated structured mesh of 0.5 in. was chosen within the connection region while a mesh size of 3 in. was chosen outside of the connection region to save on computational

expense. A refined mesh region was considered to be 18 in. from the column flanges for the beams and 18 in. from the highest and lowest beam flanges. Figure 9 shows the general mesh sizes considered in the parametric study, with the refined mesh within the connection region.

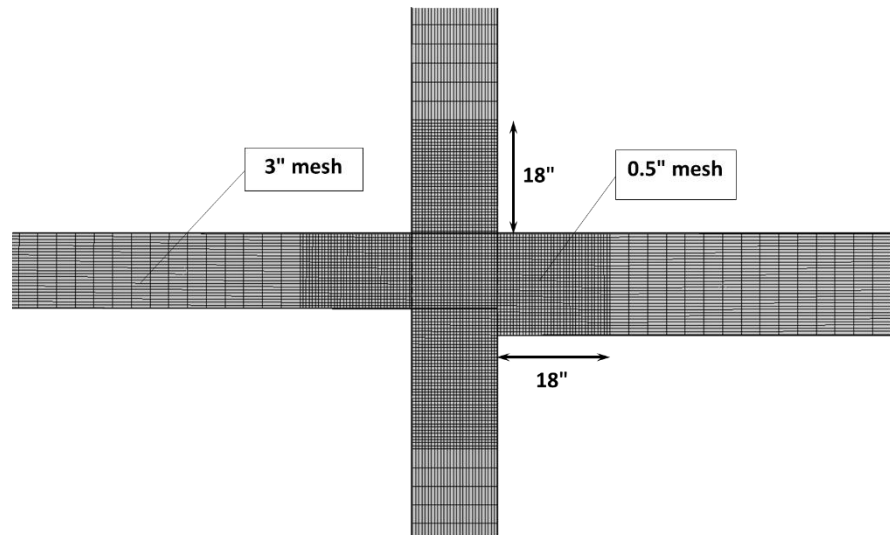


Figure 9. Mesh sizes considered in the parametric study

Boundary conditions chosen for the simulation were intended to represent restraints present at curvature inflection points within continuous building framing. Figure 10 shows the various translational and rotational degrees of freedom considered in the analyses. Given the configuration splice points were taken at the inflection points, the top and bottom of the column section are essentially pinned, with the column top allowed to translate in-plane to apply cyclic rotations to the beam-column connections. At the beam ends, rollers allow longitudinal translation while preventing rotation about the y-axis (as shown in Figure 10). Lateral restraints along the beam length are provided as typical gravity framing exists to prevent lateral beam distortions in the x-direction.

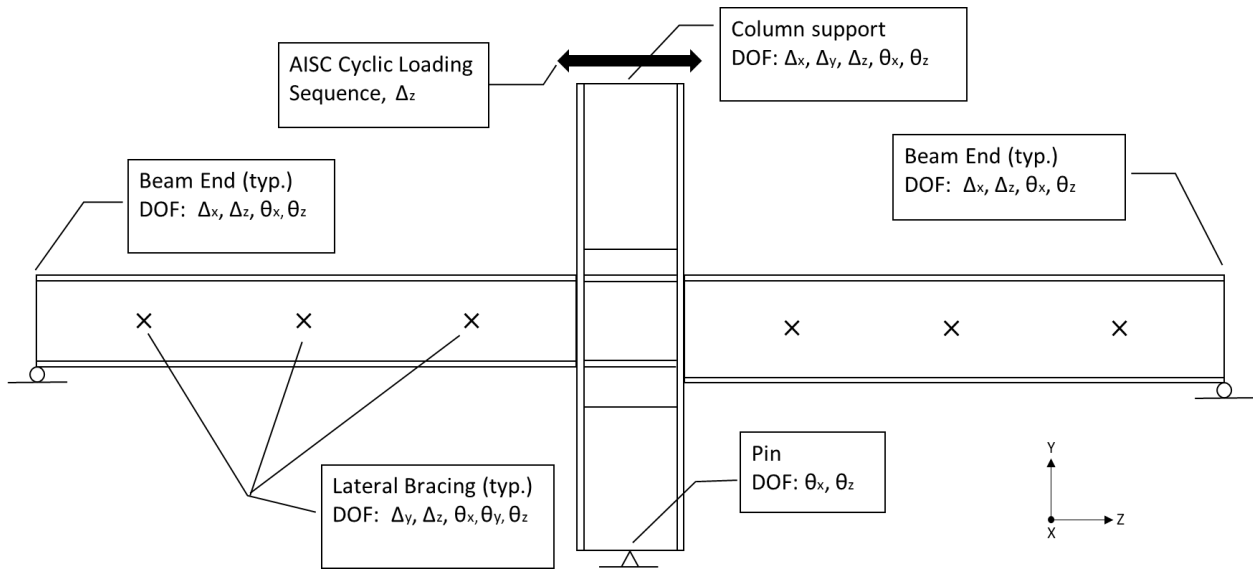


Figure 10. Boundary conditions for the two-way moment connection models

To prevent unrealistically high connection capacity due to the inherent “perfect” geometry of the simulations, all configurations were modeled with initial imperfections corresponding to the maximum allowable straightness tolerance of $L/1000$ specified in the AISC Code of Standard Practice [20]. These initial imperfections were created by scaling the fundamental buckled mode shape of each connection configuration geometry to corresponded to the maximum allowable tolerance, similar to [21].

3. Validation of Modeling Techniques

To validate the modeling techniques proposed for the parametric investigation, simulations of the experimental eccentric stiffener tests in [5] were performed and compared with the experimental results. Two column stub sections were modeled in the validation study, representing the W12x40 and W14x61 sections tested, each 4 ft. in length and had varying degrees of eccentricity. Similar to the parametric modeling approach, each column stub was modeled with four-node shell elements having reduced integration (S4R in ABAQUS). A36 steel material properties were used since the experiments in [5] were conducted prior to the implementation of

A992 steel in wide flange sections. Considered elastic material properties include the modulus of elasticity, E , equal to 29,000 ksi and Poisson's Ratio, ν , of 0.3. The yield strength was taken as 36 ksi and the ultimate strength was assumed as 58 ksi relating to standard material properties. Plastic hardening values obtained from a generalized stress-strain curve for A36 steel were considered [22]. Table 3 presents the stress and strain values used for the A36 plastic hardening model.

Table 3. Stress-strain input values for finite element modeling

| Stress (ksi) | Plastic Strain (in/in) |
|--------------|------------------------|
| 36 | 0 |
| 36 | 0.013759 |
| 42 | 0.048759 |
| 50 | 0.098759 |
| 56 | 0.148759 |
| 58 | 0.198759 |

Each of the ten test configurations from [5] were modeled with boundary conditions representative of the original experimental setup. Figure 11 shows the considered boundary conditions for the validation testing. Because the experiments used 7x0.5 in. thick bars welded to the flanges to simulate beam flange loads, boundary conditions were applied to a reference point with a rigid body constraint that enabled the displacement to be applied uniformly to a 7x0.5 in. thick surface (see Figure 11).

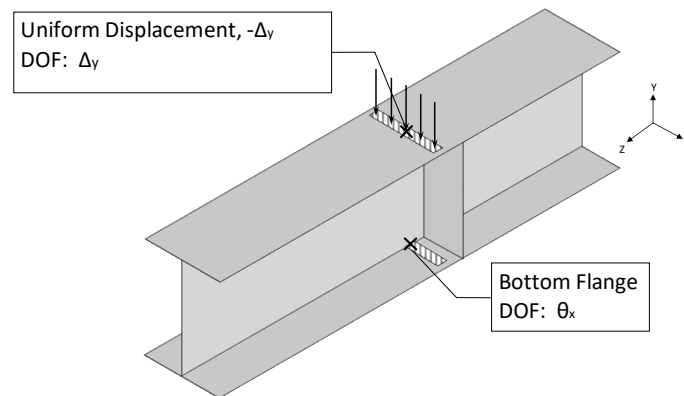


Figure 11. Boundary conditions and degrees of freedom for the modeling technique validation tests

Similar to the modeling techniques used for the parametric investigation, geometric imperfections were considered in the validation simulations; however, given the short geometry of the column stubs, different levels of scaling to the maximum allowable tolerance were considered. For example, one simulation considered “perfect” geometry in which no geometric imperfections, while three additional simulations introduced imperfections at 100%, 50%, and 10% of the maximum allowable fabrication tolerance allowed by AISC [20]. Figure 12 shows a representation of the buckled mode shape used for the initial imperfection scaling. Results from the validation simulations and parametric investigation are presented in the following results section.

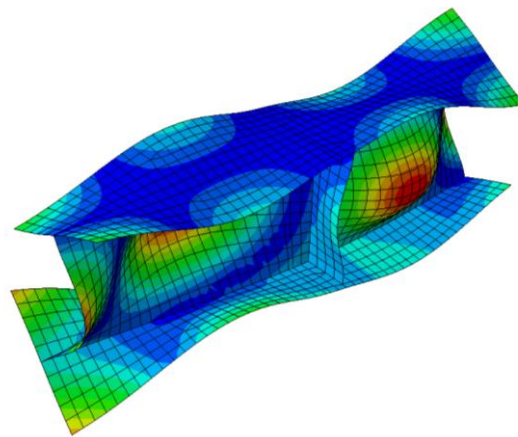


Figure 12. Frequency analysis on a column stub with continuity plate. Mode shape scale factor of 5 times for visual representation.

4. Results and Discussion

4.1. Comparison of Validation Models and Experimental Results in Graham et al. [5]

Figure 13 shows the model validation results from the W14x61 column stub configuration with 0 in. eccentricity. In Figure 13, the effect of initial imperfections are evident, as the section capacity decreases with increased imperfection. Note that the simulation considering no imperfections significantly overestimates the measured stub capacity while the simulations

considering imperfections are able to reasonably estimate the maximum stub strength. In Figure 13, the simulation with 10% scaling on the maximum allowable AISC straightness tolerance best represented the experimental result, which given the short column stub length appears reasonable. All five W14x61 configurations simulated the observed experimental result of [5] within 5% error, with three of those being within 1% error. The W12x40 simulation compare favorably as well, with the exception of the configuration with no stiffener. It is unknown what caused the high percent error for the W12x40 configuration with no stiffener, as the results for the W14x61 configuration with no stiffener were as anticipated. Table 4 shows the results of the W14x61 and W12x40 validation comparisons, with the percent error between the simulation and experimental result provided.

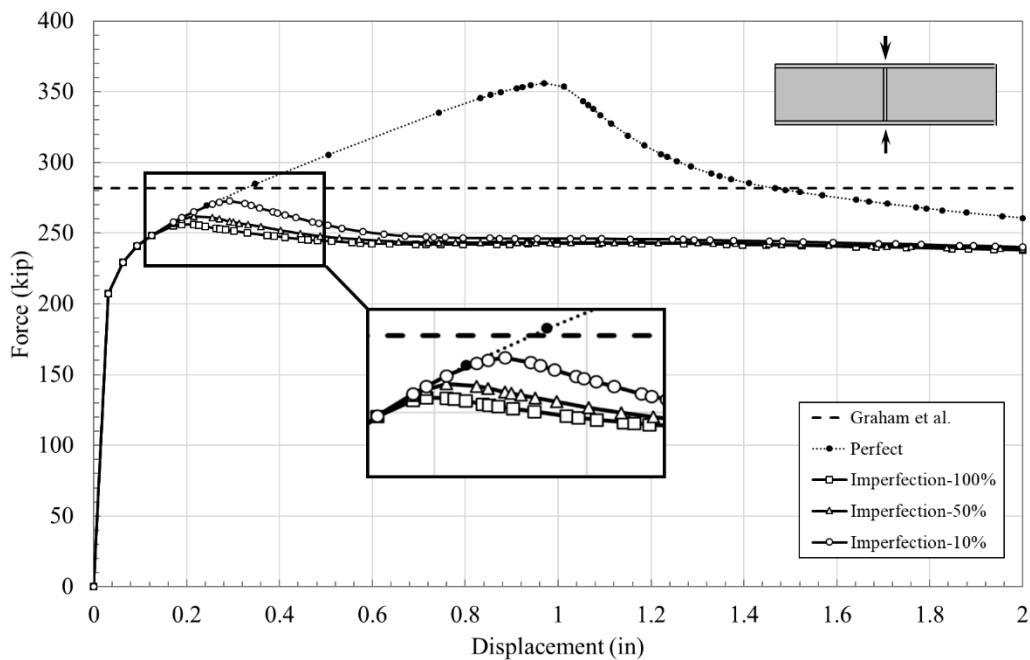


Figure 13. W14x61 column stub with 0 in. eccentricity showing the effects of scaled imperfections

Table 4. Comparison of results from Graham et al. [5] with finite element results at 10% scaled imperfections

| Column Section | Eccentricity (in) | [5] Failure Load (kips) | 10% Imperfection Failure Load (kips) | Percent Error (%) |
|----------------|-------------------|-------------------------|--------------------------------------|-------------------|
| W12x40 | 0 | 172.00 | 171.41 | 0.34% |
| W12x40 | 2 | 146.00 | 152.29 | 4.31% |
| W12x40 | 4 | 113.00 | 112.71 | 0.25% |
| W12x40 | 6 | 104.00 | 103.84 | 0.15% |
| W12x40 | NS | 102.50 | 130.63 | 27.45% |
| W14x61 | 0 | 282.00 | 272.74 | 3.28% |
| W14x61 | 2 | 232.50 | 231.63 | 0.37% |
| W14x61 | 4 | 167.60 | 166.28 | 0.79% |
| W14x61 | 6 | 142.80 | 143.14 | 0.24% |
| W14x61 | NS | 137.50 | 143.33 | 4.24% |

From Table 4, the results of the finite element analysis compared favorably with the measured failure loads from [5]. Figure 14 compares a photograph of the deformed shape during testing to the finite element results of the same section. From Figure 14, the flange deformation appears similar, and both have significant local yielding in the web at the applied force location. Comparing the model and experimental results presented in Table 4, along with visual comparisons between documented deformations during testing, confidence in the chosen modeling techniques to simulate the eccentric moment connection configurations in the parametric investigation was reasonably achieved.

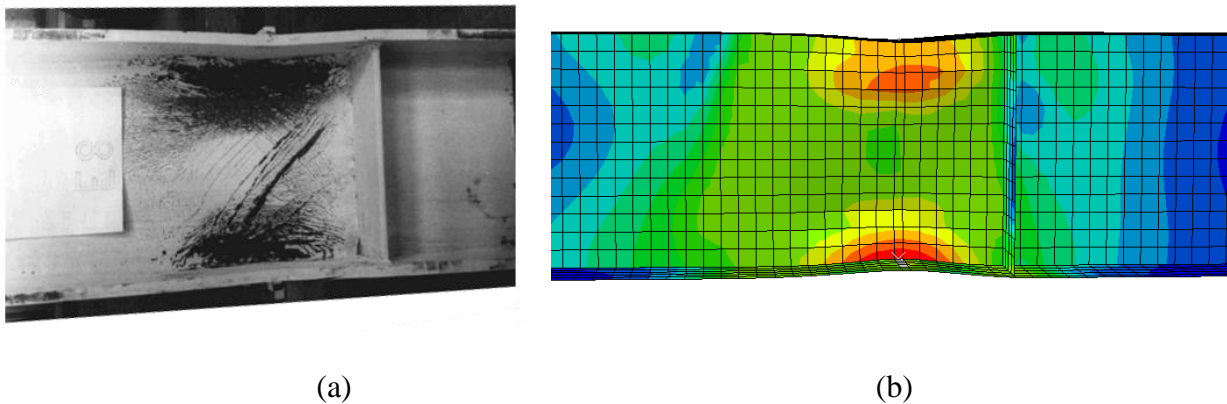


Figure 14. Comparison of the (a) results of [5] to the (b) finite element results

4.2. General Observations from the Parametric Simulations

For the configurations considered in the parametric investigation, local failure was isolated to FLB; however, significant column flange yielding (yielding of the entire column flange cross-section) was observed prior to the FLB limit state (see Figure 15 and Figure 16). Given this observed yielding, and with capacity based design principles often aiming to prevent significant column damage, an additional failure mode of flange local yielding (FLY) was developed. FLY indicates complete yielding of the column flange section, was created and investigated in the connection analyses. Figure 15 shows a typical observation of yielding within the column flange sections following rotations at 0.03 rad in the cyclic loading protocol. Additionally, Figure 16 shows the von Mises stress distributions at the FLY failure increment for the same configuration as shown in Figure 15.

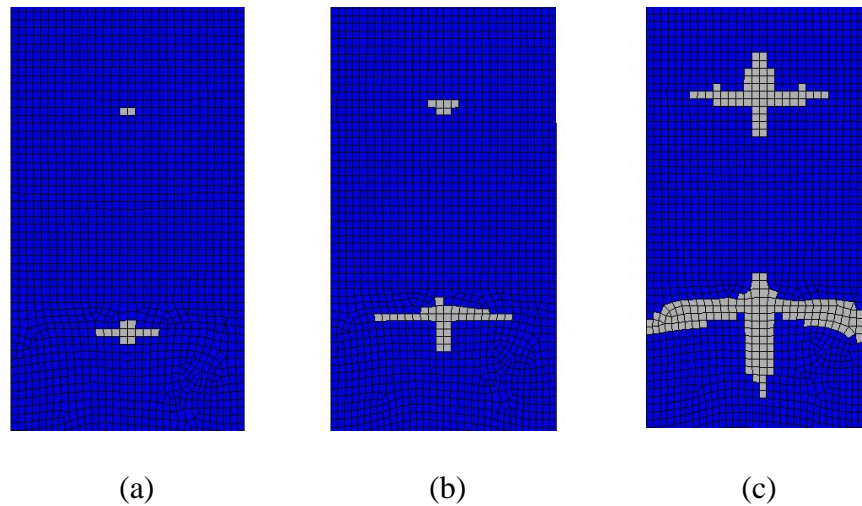


Figure 15. Progression of PEEQ (plastic equivalent strain) on column flange at location of beam flanges for the 1.645 eccentric connection (a) 1st cycle, 0.02 rad. (b) 2nd cycle, 0.02 rad. (c) 1st cycle, 0.03 rad.

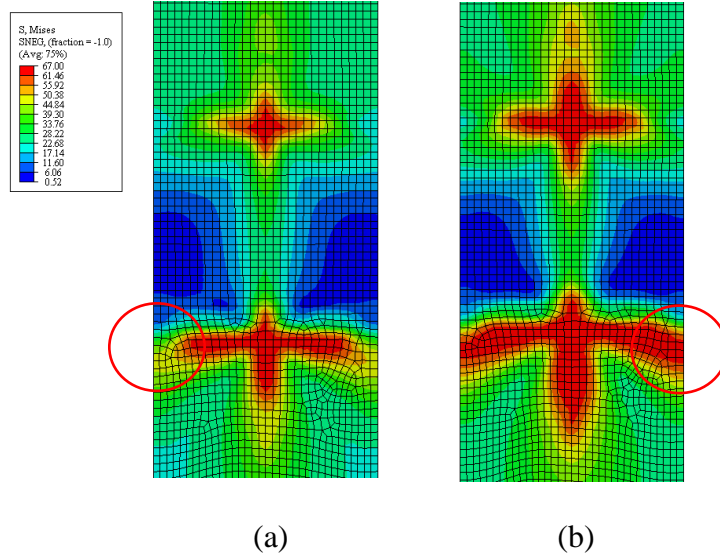


Figure 16. Determining column flange yield increment using Von Mises stress (a) Increment 526 (b) Increment 527 (0.03 rad.)

The average FLY failure load for the W14x132 configurations was 428.5 kips and the column flange on the side with the deeper beam and continuity plate eccentricity failed first, as expected. The average FLY failure load for the W21x147 configurations was 481 kips. For the W21x147 column configurations, the FLY limit often occurred on both flanges of the column simultaneously.

Figure 17 shows the standard deviation plots of the FLY values for the un-stiffened W14x132 column and the W21x147 column configurations respectively. From Figure 17, over half of the FLY capacity values for the W14x132 column were within one standard deviation of the average and almost two-thirds of the FLY values for the W21x147 column were within one standard deviation. Given the variation in beam flange size amongst the configurations and initial imperfections being applied, using an average FLY limit state was deemed appropriate for making strength comparisons with the eccentric connection simulations.

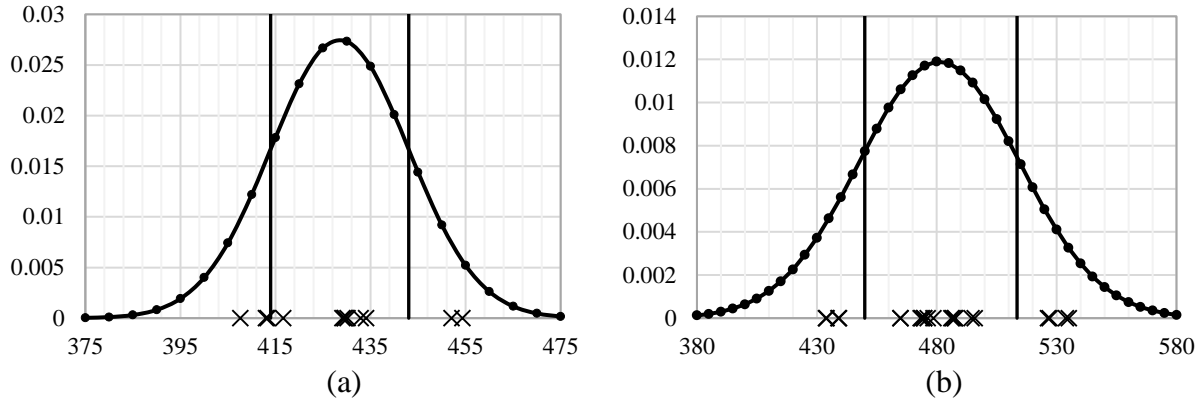


Figure 17. Standard deviation plots for FLY limit state (a)W14x132 (b)W21x147

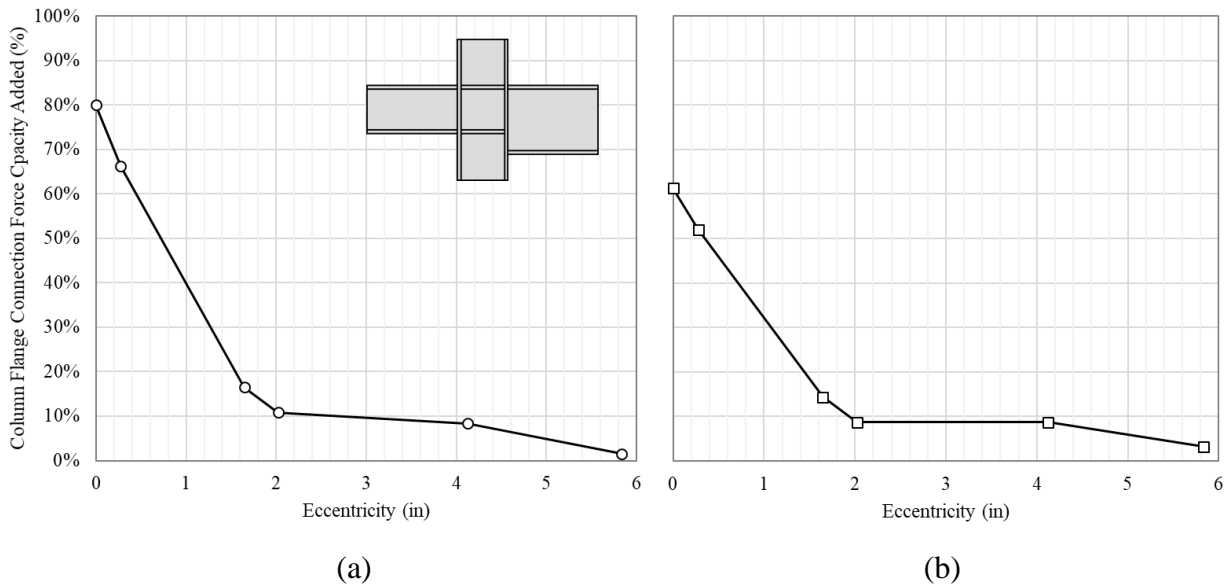
The available strength for the FLB limit state according to the design strength equation from [1], for the W14x132 column sections and the W21x147 column sections was 298.4 kips and 372.0 kips, respectively. The W14x132 column section had an average FLB capacity of 502 kips and the W21x147 had an average FLB capacity of 559.2 kips. Comparing the average FLB capacities to the FLB equation in [1] indicates it is rather conservative for these column sections. It is possible that higher amounts of strain hardening occur as a result of the cyclic loading associated with seismic design, leading to higher capacities for FLB.

4.3. Effect of Eccentricity on Continuity Plate Strength Contribution

As expected, increasing eccentricity between the beam flange and continuity plate results in decreased continuity plate participation. Figure 18 shows results from the parametric analyses comparing the amount of connection eccentricity versus the participation of the continuity plate to connection strength. Figure 18(a) and (b) plot the continuity plate strength contribution up to complete yielding of the column flange (the FLY limit state discussed earlier). Figure 18(c) and (d) show the continuity plate strength contribution up to a column flange deformation of $\frac{1}{8}$ in. (the FLB limit state discussed earlier). Note that the ordinate value of 0% in Figure 18 corresponds to the unstiffened column flange strength (no continuity plate strength contribution).

For the FLY consideration in Figure 18(a) and (b), there is a steep decline in continuity plate contribution within eccentricities ranging from 0 to 2 in. Added strength by the continuity plates for both column sections diminished to around 10% at 2 in. eccentricity. For connections having eccentricities greater than 2 in., both column sections receive a 10% contribution from the continuity plates until reducing to essentially the unstiffened configuration at an eccentricity of 6 in.

The continuity plate contribution considering the FLB limit state which allows larger column flange deformations, noticed a near linear decline from between 40-50% strength added while in-line to 0% strength added at a 6in. eccentricity. In Figure 18(c) and (d), the continuity plate contribution reduces to 10% at an eccentricity of 4in, while 30-40% strength added still remains at eccentricities greater than 2 in. In the current specifications, no contribution from the continuity plate is recommended after an eccentricity of 2 in.



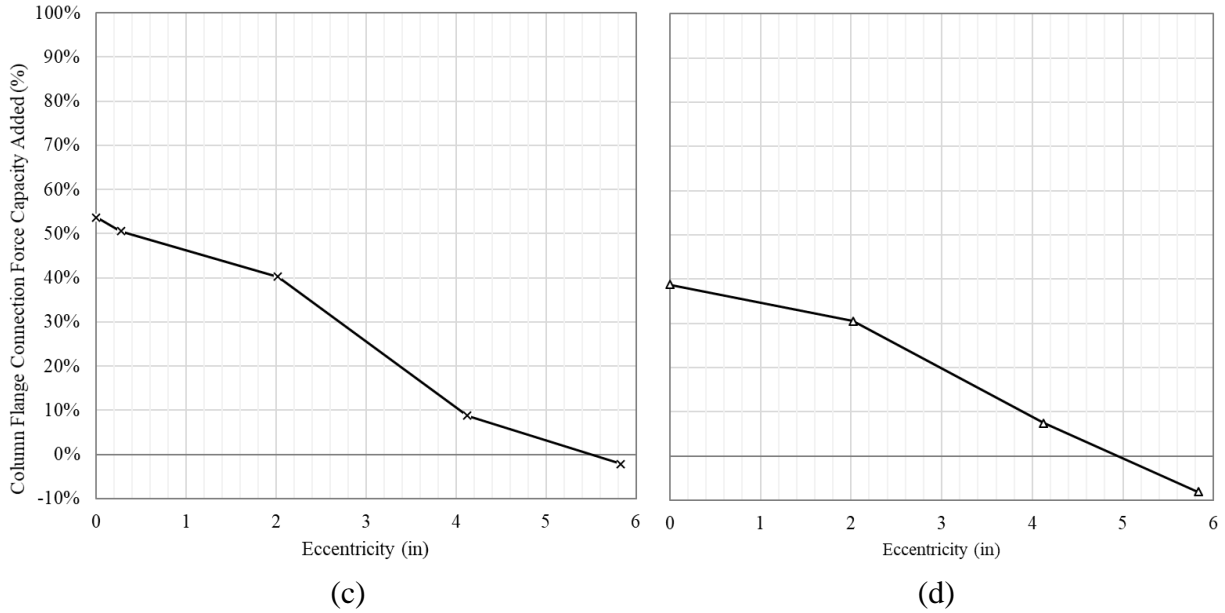


Figure 18. Column flange connection force capacity added with respect to eccentricity for (a) W14x132 FLY (b) W21x147 FLY (c) W14x132 FLB (d) W21x147 FLB

Figure 19 shows the flange stress distributions for the W14x132 column section at each configuration eccentricity considered. All flange stress plots in Figure 19 are taken at the second cycle of 0.04 rad. Note in Figure 19 that following a flange eccentricity of 0.275 in (nearly in-line) complete yielding of the column flange section occurs prior completing the 0.4 rad cycles. If column FLY is a concern for designers, it should be expected that a column flange section having any beam eccentricity would completely yield during a seismic event.

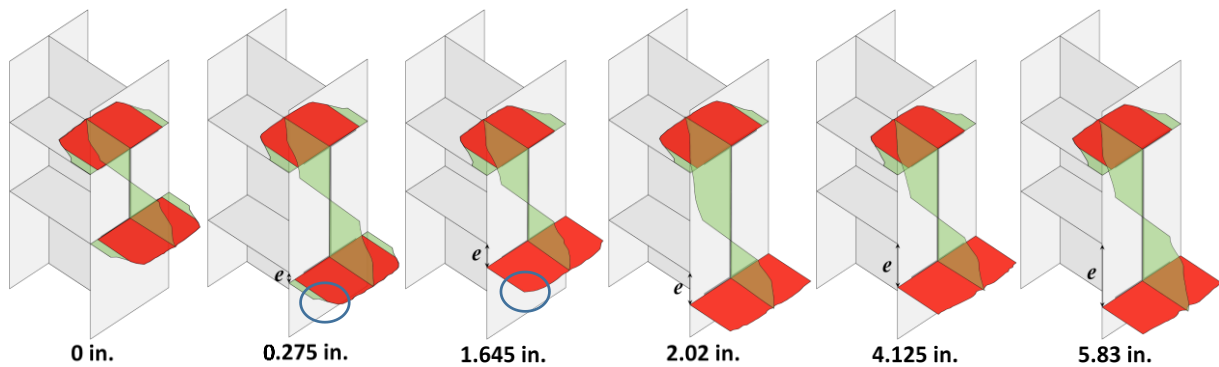


Figure 19. Stresses on W14x132 column flange at 2nd cycle, 0.04 rad. as eccentricity increases

Figure 20 compares the continuity plate contribution during the FLY and FLB limit states with the results obtained from experimental testing by Graham et al. [5]. In Figure 20, the observed trends considering flange local bending match well with those observed in the testing by [5]. Note that the experiments in [5] used weld fracture as the indicator of failure, which is more closely associated with the flange deformation limit (FLB) than with plastic straining of the column flange. It should also be noted that the W14x132 column has a similar width-to-thickness ratio ($b/2t_f = 7.15$) as the W12x40 section used by [5] ($b/2t_f = 7.77$), somewhat explaining the consistencies between the two curves. Additionally, the W14x61 ($b/2t_f = 7.75$) section used by [5] considered a thicker continuity plate than the W12x40 section ($3/4$ in. thick compared to $1/2$ in. thick), explaining why the connection force added by the continuity plate is much higher than the W12x40 section.

For the connections with an eccentricity of 2.02 in., the FLY limit state indicated that the continuity plate would add approximately 10% of the connection force whereas the FLB limit state indicated the continuity plate would add nearly 40%. See Appendix A3 for the complete hysteretic connection response at various eccentricity levels.

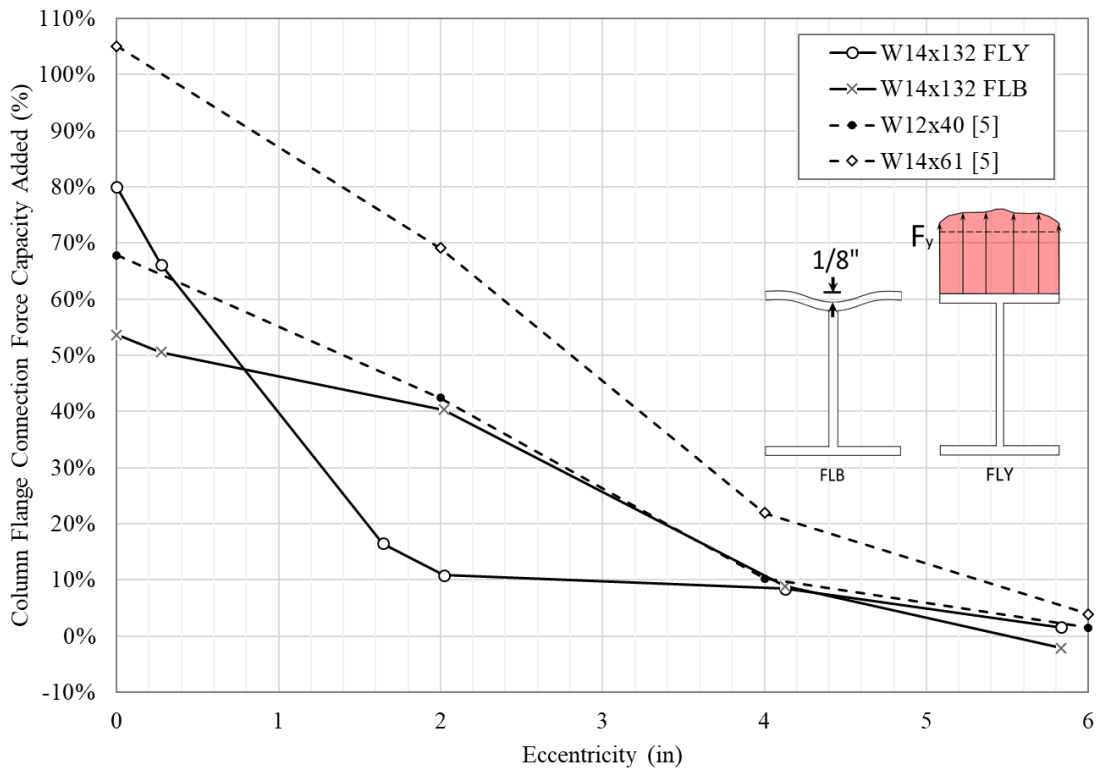


Figure 20. Impact of selection of criteria for FLB limit state on the column flange connection force capacity added

Table 5 shows the flange forces required to reach both the FLY and FLB limit states. The flange forces for both the inline connections are denoted with an asterisk in Table 5 because they correspond to the maximum beam flange force for these configurations. Unlike the eccentric configurations, the in-line connections did not exhibit the observed pattern of yielding shown previously in Figure 15. This is to be expected, as these connections are considered properly stiffened and designed according to applicable design code standards considering these limit states. In Table 5, the in-line flange forces acting on each column are considered as the maximum beam flange force that can be delivered to the column flange.

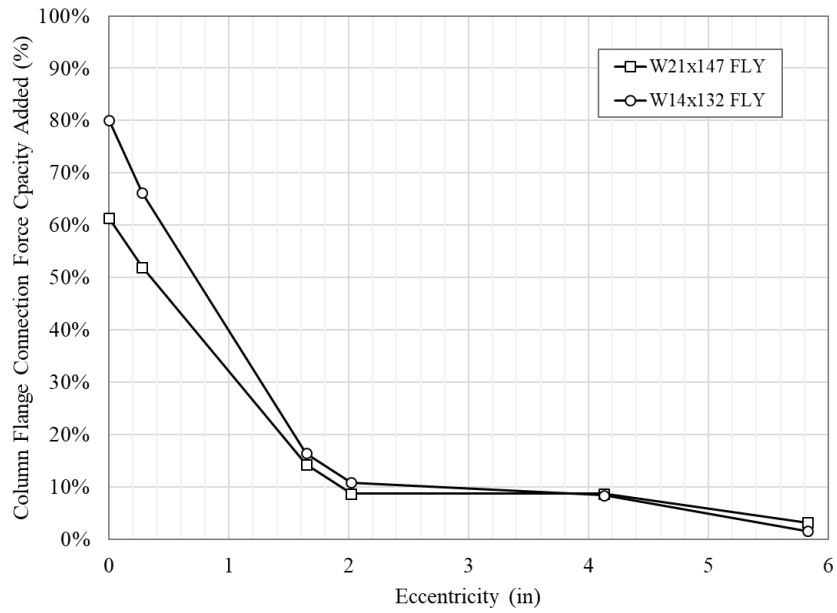
Table 5. Flange forces at FLY and FLB limit state for W14x132 column section

| Column | Beam 1 | Eccentricity (in) | P _r FLY (kips) | Drift at FLY Failure (rad) | P _r FLB (kips) | Drift at FLB Failure (rad) | P _r 0.8M _p (kips) |
|---------|---------|-------------------|---------------------------|----------------------------|---------------------------|----------------------------|---|
| W14x132 | W12x96 | 0.000 | 771.3 | (1) 0.07 | 771.3* | (1) 0.07 | 591.3 |
| W14x132 | W16x100 | 0.275 | 712.0 | (1) 0.05 | 755.8 | (1) 0.07 | 615.2 |
| W14x132 | W14x82 | 1.645 | 499.0 | (1) 0.03 | - | - | 493.9 |
| W14x132 | W18x106 | 2.020 | 475.0 | (1) 0.02 | 704.2 | (1) 0.06 | 629.3 |
| W14x132 | W16x89 | 4.125 | 464.5 | (1) 0.03 | 546.3 | (1) 0.05 | 515.7 |
| W14x132 | W18x86 | 5.830 | 435.2 | (1) 0.03 | 491.2 | (1) 0.04 | 475.1 |
| W21x147 | W12x96 | 0.000 | 776.1* | (1) 0.06 | 776.1* | (1) 0.06 | 594.1 |
| W21x147 | W16x100 | 0.275 | 731.3 | (1) 0.05 | - | - | 612.9 |
| W21x147 | W14x82 | 1.645 | 550.0 | (1) 0.03 | - | - | 497.7 |
| W21x147 | W18x106 | 2.020 | 522.9 | (1) 0.02 | 729.7 | (1) 0.06 | 631.7 |
| W21x147 | W16x89 | 4.125 | 522.8 | (1) 0.03 | 600.8 | (1) 0.05 | 530.1 |
| W21x147 | W18x86 | 5.830 | 496.3 | (1) 0.03 | 513.8 | (1) 0.04 | 491.6 |

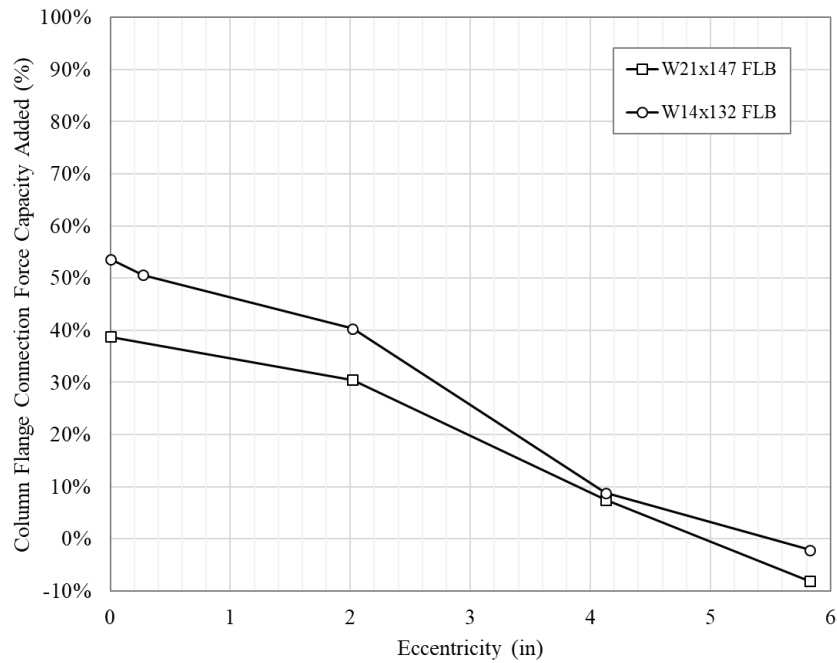
4.4. Effect of Width- Thickness Ratio on Continuity Plate Participation

The W14x132 section and the W21x147 were selected so as to vary the width-to-thickness ratios of the column sections. The limiting width-to-thickness ratio for the flanges of the selected columns was 7.35, based on the compactness requirements in the seismic provisions. The W14x132 column has a $b/2t_f$ ratio of 7.15, and was chosen as an upper bound for column slenderness. The W21x147 column section was selected to investigate a more compact section and help determine slenderness effects on allowable connection eccentricity. The W21x147 column has a $b/2t_f$ ratio of 5.44.

More compact sections receive less contribution from continuity plates, regardless of the limit state. Figure 21 again compares the two column sections for the FLY and FLB limit states to contrast slenderness effects. Figure 21(a) demonstrates a shift in continuity plate contribution for the FLY limit considered, with higher slenderness resulting in higher contribution from the continuity plates. This shift is most evident when the eccentricity is less than 2 inches. For the FLB limit state, Figure 21(b) a similar slenderness trend is observed; however, this trend extends beyond the 2 in. eccentricity.



(a)



(b)

Figure 21. Impact of width-to-thickness ratios of columns on effectiveness of eccentric continuity plates for (a) FLY limit state and (b) FLB limit state

4.5. Design Recommendations

The current design recommendations for allowable eccentricity reduce continuity plate contributions as the beam-flange-to-continuity-plate eccentricity increases. The recommendations in [3] state, “...provided the strength [in an eccentric connection] be reduced linearly from 100% at zero eccentricity to 65% at 2 in. eccentricity.” Equation 3 represents this recommendation which reduces the in-line connection capacity by 35% at an eccentricity of 2 in. Beyond 2 in., the current recommendations account for no contribution from the continuity plates. In Equation 3, $R_{u,st}$ represents the required strength of the continuity plates (the difference between the concentrated force being applied and the allowable strength of the column flange according to the FLB limit state).

$$\phi R_{n,ecc} = \phi R_{n,FLB} + \left(R_{u,st}(1 - 0.175e) \right) \quad 0 \text{ in.} \leq e \leq 2 \text{ in.} \quad \text{Eqn-3}$$

With the results of the parametric study indicating continuity plate contribution at eccentricities greater than 2 in., a new design equation for calculating connection capacity at eccentricities up to 4.5 in. was developed. Based on the continuity plate contributions determined from the parametric investigation, Equation 4 was developed to calculate resulting connection capacity ($\phi R_{n,ecc}$). The proposed equation provides connection capacities for eccentricities up to 4.5 in., after which no contribution of the continuity plate is assumed. Figure 22 shows the current and proposed continuity plate contributions from Equations 3 and 4 (governed by the FLB limit state) versus the considered connection eccentricity. Also shown in Figure 22 are the values obtained from the parametric study for comparison.

$$\phi R_{n,ecc} = \phi R_{n,FLB} + R_{u,st}(-0.039(e^2 + e - 25)) \quad 0 \text{ in.} \leq e \leq 4.5 \text{ in.} \quad \text{Eqn-4}$$

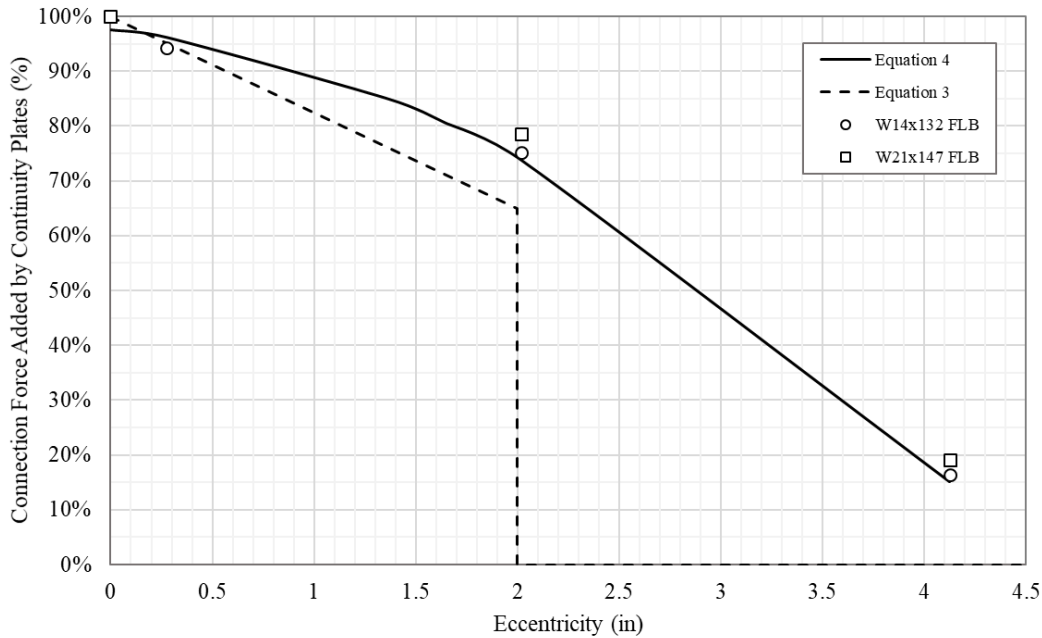


Figure 22. Connection force added by continuity plates for FLB limit state

It is proposed that Equation 4 be used for concentrated forces, given that the following requirement is met: the connection is designed with sufficient available strength for the continuity plates in areas in which the stiffening action will be inline. This differs from the other limit states in Section J10 of [1], as it is intended to be checked after inline continuity plates have been designed and only for cases of eccentric continuity plates.

Inline continuity plates essentially enable the column to increase its concentrated force capacity by increasing stiffness at the location of the force. This research has shown that when these continuity plates are at an eccentricity from the concentrated force, continuity plates still provide increased stiffness, just at a reduced amount. Equation 4 is designed to predict the effectiveness of the continuity plates in their ability to increase the column flange capacity for concentrated forces. It should be noted the equations are designed to be conservative, using the required strength of the continuity plates rather than the available strength because of possible variation in size of continuity plates.

Appendix A4 shows the complete proposed process of designing for eccentric continuity plates using Equation 4.

5. Conclusions

In this study, a parametric finite element investigation was conducted to investigate continuity plate contributions in steel beam-to-column connections having eccentricities. A total of 12 detailed finite element analyses considering two column sections (W14x and W21x sections) and six levels of connection eccentricity (ranging from 0 to 6 in.) were considered. Modeling techniques considered for the parametric investigation were validated against experiments performed by others. The following conclusions are based on the analytical parametric investigation.

- 1) Complete yielding of the column flange cross-section occurs prior to the code flange local bending limit state. If column flange local yielding is a concern for designers, it should be expected that a column flange section having any beam eccentricity would completely yield during a seismic event.
- 2) As expected, increasing the level of eccentricity between the beam flange and continuity plate results in decreased continuity plate participation; however, unlike current code recommendations, significant participation (up to 10% additional flange capacity for a W14x132 column) was observed for eccentricities up to 4 in.
- 3) More compact column sections receive less contribution from continuity plates, regardless of the limit state. The effect of beam flange eccentricity on column capacity is reduced as sections become more compact.
- 4) A new design equation for determining beam-to-column connection capacities is proposed, extending continuity plate contributions for eccentricities up to 4.5 in.

6. References

1. AISC, *Specification for Structural Steel Buildings*. 2016, American Institute of Steel Construction: Chicago, IL.
2. Segui, W.T., *Steel Design*. 2013, Stamford, CT: Cengage Learning.
3. Carter, C.J., *Stiffening of Wide-Flange Columns at Moment Connections: Wind and Seismic Applications, Design Guide 13*. 1999, Chicago, IL.: AISC.
4. AISC, *Seismic Provisions for Structural Steel Buildings*. 2016, American Institute of Steel Construction: Chicago, IL.
5. Graham, J.D., Shearbourne, A.N., Khabbaz R.N., and Jensen, C.D., *Welded Interior Beam-to-Column Connections*. AISC Report, 1959.
6. AISC, *Prequalified Connections for Special and Intermediate Steel Moment Frames for Seismic Applications*. 2016, AISC: Chicago, IL.
7. Hajjar, J.F., Dexter, Robert J., Ojard, Sara D., Ye, Yanqun, Cotton, Sean C., *Continuity Plate Detailing for Steel Moment-Resisting Connections*. Engineering Journal, 2003. Fourth Quarter.
8. Prochnow, S.D., Dexter, Robert J., Hajjar, Jerome F., Ye, Yanqun, Cotton, Sean C., *Local Flange Bending and Local Web Yielding Limit States in Steel Moment-Resisting Connections*, in *Structural Engineering Report*. 2000, University of Minnesota: Minneapolis, MN.
9. ASTM, *Standard Specification for General Requirements for Rolled Structural Steel Bars, Plates, Shapes, and Sheet Piling*. 2017, ASTM International: West Conshohocken, PA.
10. Lee, D., Cotton, Sean C., Dexter, Robert J., Hajjar, Jerome F., Ye, Yanqun, Ojard, Sara D., *Column Stiffener Detailing and Panel Zone Behavior of Steel Moment Frame Connections*, in *Structural Engineering Report*. 2002, University of Minnesota: Minneapolis, MN.
11. Jones, S.L., Fry, Gary T., Engelhardt, Michael D. , *Experimental Evaluation of Cyclically Loaded Reduced Beam Section Moment Connections*. Journal of Structural Engineering, 2002. April 2002.
12. Roeder, C., Coons, Russell G., Hoit, Mathew, *Simplified Design Models for Predicting the Seismic Performance of Steel Moment Frame Connections*, in *SAC Joint Venture*. 2000, University of Washington.

13. Sumner, E.A., Mays, Timothy W., Murray, Thomas M. , *Cyclic Testing of Bolted Moment End-Plate Connections*, in *SAC Joint Venture*. 2000, Virginia Polytechnic Institute and State University.
14. Venti, M.J., Engelhardt, Michael D., *Test of a Free Flange Connection with a Composite Floor Slab*, in *SAC Joint Venture*. 2000, University of Texas at Austin.
15. Zhang, X., Ricles, James M., *Experimental Evaluation of Reduced Beam Section Connections to Deep Columns*. *Journal of Structural Engineering*, 2006. March 2006.
16. Zhang, X., Ricles, James M., *Seismic Behavior of Reduced Beam Section Moment Connections to Deep Columns*. *Journal of Structural Engineering*, 2006. March 2006.
17. *ABAQUS ABAQUS/CAE User's Guide Ver. 6.14*, Dassault Systemes Simulia Corp. 2014.
18. AISC, *Steel Construction Manual*. 2017, American Institute of Steel Construction: Chicago, IL.
19. Kaufmann, E.J., Metrovich, B.R., Pense, A.W., *Characterization of cyclic inelastic strain behavior on properties of A572 Gr. 50 and A913 Gr. 50 rolled sections*, in *ATLSS Rep. No. 01-13*. 2001, National Center for Engineering Research on Advanced Technology for Large Structural Systems, Lehigh University, Bethlehem, PA.
20. AISC, *Code of Standard Practice for Steel Buildings and Bridges*. 2016, AISC: Chicago, IL.
21. Desrochers, C., *Effect of Column Axial Load on Skewed SMF RBS Connection Demands*. 2017, University of Arkansas.
22. Turnquist, M., *Advanced Buckling Analysis of a Reactor Tank Supported by Four Legs*. *Inspectioning Journal*, 2013. 23(4).

Appendix

A1. Connection Design

Design of the connections for the parametric study met AISC Specification, AISC Seismic Provisions, and AISC Design Guide 13 requirements for special moment frames. The design procedure for the W14x132 column with 1.645 in. eccentricity (W12x96 and W14x82 beams) is detailed in this appendix and is representative of the procedure used for all of the connections. Subscripts “c”, “b1”, “b2”, and “st” denote column, beam 1, beam 2, and stiffener, respectively.

Column Properties

Try W14x132

$$\begin{array}{lllll}
 A_g := 38.8 \cdot \text{in}^2 & d := 14.7 \cdot \text{in} & Z_x := 234 \cdot \text{in}^3 & Z_y := 113 \cdot \text{in}^3 & r_x := 6.28 \cdot \text{in} \\
 r_y := 3.76 \cdot \text{in} & l := 13 \cdot \text{ft} & F_y := 50 \cdot \text{ksi} & F_u := 65 \cdot \text{ksi} & E := 29000 \cdot \text{ksi} \\
 K_x := 1.2 & K_y := 1.0 & b_{fc} := 14.7 \cdot \text{in} & t_{fc} := 1.03 \cdot \text{in} & \\
 h := 11.44 \cdot \text{in} & t_{wc} := 0.645 \cdot \text{in} & k := 1.63 \cdot \text{in} & R_y := 1.1 &
 \end{array}$$

$$\frac{b_{fc}}{2 \cdot t_{fc}} = 7.14 \quad 0.32 \cdot \sqrt{\frac{E}{R_y \cdot F_y}} = 7.35 \quad 7.14 \leq 7.35 \quad \text{OK}$$

$$\frac{h}{t_{wc}} = 17.74 \quad 2.57 \cdot \sqrt{\frac{E}{R_y \cdot F_y}} \cdot (1 - (1.04 (5\%))) = 55.945 \quad 17.74 \leq 55.95 \quad \text{OK}$$

∴ W14x132 column meets seismic compactness requirements as a highly ductile member
(see AISC Seismic Provisions Table D1.1)

Note: assumed an axial force of 5% of the column design strength

$$\max\left(\frac{K_x \cdot l}{r_x}, \frac{K_y \cdot l}{r_y}\right) = 41.5 \quad F_e := \frac{\pi^2 \cdot E}{\left(\max\left(\frac{K_x \cdot l}{r_x}, \frac{K_y \cdot l}{r_y}\right)\right)^2} = 166.3 \text{ ksi}$$

$$\frac{F_y}{F_e} = 0.301 \quad 0.301 \leq 2.25 \quad \text{use AISC Specification Eq. E3-2}$$

$$F_{cr} := \left(0.658^{\frac{F_y}{F_e}}\right) \cdot F_y = 44.1 \text{ ksi}$$

$$\phi := 0.9 \quad \phi P_n := \phi \cdot F_{cr} \cdot A_g = 1539.5 \text{ kip}$$

$$M_{pc} := Z_x \cdot \left(F_y - \frac{0.05 \cdot \phi P_n}{A_g}\right) = 11235.8 \text{ kip} \cdot \text{in}$$

Beam Properties

Try W12x96 and W14x82

W12x96 (Beam 1)

$$\begin{array}{lllll}
 d_{bl} := 12.7 \cdot \text{in} & l := 15 \cdot \text{ft} & h := 9.74 \cdot \text{in} & Z_x := 147 \cdot \text{in}^3 & w := 96 \cdot \frac{\text{lb}}{\text{ft}} \\
 b_{fl} := 12.2 \cdot \text{in} & t_{fl} := 0.9 \cdot \text{in} & t_{wbl} := 0.55 \cdot \text{in} & &
 \end{array}$$

$$C_{pr} := \frac{F_y + F_u}{2 \cdot F_y} = 1.15$$

$$w := 96 \cdot \frac{\text{lb}}{\text{ft}} \quad 96 \cdot \frac{\text{lb}}{\text{ft}} \leq 150 \cdot \frac{\text{lb}}{\text{ft}}$$

$$t_{fb1} = 0.9 \text{ in} \quad 0.9 \cdot \text{in} \leq 1 \cdot \text{in}$$

$$\frac{l}{d} = 12.24 \quad 14.17 \geq 7$$

$$\frac{b_{fb1}}{2 \cdot t_{fb1}} = 6.78 \quad 0.32 \cdot \sqrt{\frac{E}{R_y \cdot F_y}} = 7.35 \quad 6.78 \leq 7.35 \quad \text{OK}$$

$$\frac{h}{t_{wb1}} = 17.71 \quad 2.57 \cdot \sqrt{\frac{E}{R_y \cdot F_y}} = 59.013 \quad 17.71 \leq 55.95 \quad \text{OK}$$

∴ W12x96 column meets seismic compactness requirements as a highly ductile member
(see AISC Seismic Provisions Table D1.1)

$$M_{pb1} := R_y \cdot C_{pr} \cdot F_y \cdot Z_x = 9297.8 \text{ kip} \cdot \text{in}$$

Note: neglecting moment due to shear amplification because plastic hinge will be located at the column flange

W14x82 (Beam 2)

$$d_{b2} := 14.3 \cdot \text{in} \quad l := 15 \cdot \text{ft} \quad h := 11.42 \cdot \text{in} \quad Z_x := 139 \cdot \text{in}^3 \quad w := 82 \cdot \frac{\text{lb}}{\text{ft}}$$

$$b_{fb2} := 10.1 \cdot \text{in} \quad t_{fb2} := 0.855 \cdot \text{in} \quad t_{wb2} := 0.51 \cdot \text{in}$$

$$C_{pr} := \frac{F_y + F_u}{2 \cdot F_y} = 1.15$$

$$w = 82 \frac{\text{lb}}{\text{ft}} \quad 82 \cdot \frac{\text{lb}}{\text{ft}} \leq 150 \cdot \frac{\text{lb}}{\text{ft}}$$

$$t_{fb2} = 0.855 \text{ in} \quad 0.9 \cdot \text{in} \leq 1 \cdot \text{in}$$

$$\frac{l}{d} = 12.24 \quad 12.59 \geq 7$$

$$\frac{b_{fb2}}{2 \cdot t_{fb2}} = 5.91 \quad 0.32 \cdot \sqrt{\frac{E}{R_y \cdot F_y}} = 7.35 \quad 5.91 \leq 7.35 \quad \text{OK}$$

$$\frac{h}{t_{wb2}} = 22.39 \quad 2.57 \cdot \sqrt{\frac{E}{R_y \cdot F_y}} = 59.013 \quad 22.39 \leq 55.95 \quad \text{OK}$$

∴ W14x82 column meets seismic compactness requirements as a highly ductile member
(see AISC Seismic Provisions Table D1.1)

$$M_{pb2} := R_y \cdot C_{pr} \cdot F_y \cdot Z_x = 8791.8 \text{ kip} \cdot \text{in}$$

Strong Column - Weak Beam Check

$$\frac{\sum M_{pc}}{\sum M_{pb}} \geq 1 \quad \frac{2 \cdot M_{pc}}{M_{pb1} + M_{pb2}} = 1.242 \quad 1.242 \geq 1 \quad \text{OK}$$

Column Concentrated Force Capacities

$$R_{ub1} := \frac{0.85 \cdot M_{pb1}}{(d_{b1} - t_{fb1})} = 669.8 \text{ kip}$$

$$R_{ub2} := \frac{0.85 \cdot M_{pb2}}{(d_{b2} - t_{fb2})} = 555.8 \text{ kip}$$

$$\phi := 0.9 \quad \phi R_{nFLB} := \phi \cdot 6.25 \cdot F_y \cdot t_f^2 = 298.4 \text{ kip}$$

$$\phi := 1.0 \quad l_b := \min(t_{fb1}, t_{fb2}) = 0.855 \text{ in} \quad \phi R_{nWLY} := \phi \cdot F_y \cdot t_{wc} \cdot (5 \cdot k + l_b) = 290.4 \text{ kip}$$

Note: Since the web local yielding limit state (WLY) will be taken care of with doubler plates, use the design strength for flange local bending (FLB). The other limit states in AISC Specification J10 must be checked, however they larger than WLY and thus would not control.

$$R_{ub1} > \phi R_{nFLB} \quad \therefore \quad \text{continuity plates required}$$

Continuity Plate Design

$$R_{ust} := R_{ub1} - \phi R_{nFLB} = 371.4 \text{ kip}$$

$$\phi := 0.9 \quad F_y := 36 \cdot \text{ksi} \quad A_{smin} := \frac{R_{ust}}{\phi \cdot F_y} = 11.462 \text{ in}^2$$

$$b_{smin} := \frac{b_{fb1}}{2} - \frac{t_{wc}}{2} = 5.78 \text{ in} \quad \text{select } b_{st} \geq b_{smin}$$

$$t_{smin} := 0.75 \cdot t_{fb1} = 0.675 \text{ in} \quad \text{select } t_{st} \geq t_{smin}$$

Try 1 in. thick, full width continuity plate on both sides of column web

$$b_{st} := \frac{b_{fc}}{2} - \frac{t_{wc}}{2} = 7.03 \text{ in} \quad (\text{full column width})$$

$$t_{st} := 1 \cdot \text{in}$$

$$A_{st} := 2 \cdot b_{st} \cdot t_{st} = 14.1 \text{ in}^2 \quad A_{st} \geq A_{stmin} \quad \text{OK}$$

A2. Calculations for Column Flange and Continuity Plate Connection Force Capacity Added

Sample calculations for W14x132 column, 2.02 in. configuration

Column Flange Connection Force Capacity Added

Column Flange Concentrated Force Capacity for FLB Limit State (from unstiffened finite element results)

$$\phi R_{n,FLB} := 502 \text{ kip}$$

Beam Flange Force at FLB Limit State

$$P_{f,FLB} := 702.4 \text{ kip}$$

Percent of Column Flange Capacity Added with eccentric continuity plate

$$\frac{P_{f,FLB} - \phi R_{n,FLB}}{\phi R_{n,FLB}} = 40\%$$

Connection Force Added by Continuity Plates

Maximum Beam Flange Force (from inline configuration)

$$P_{f,FLB,max} := 771.3 \text{ kip}$$

Maximum Connection Force Added (from inline connection)

$$P_{f,FLB,max} - \phi R_{n,FLB} = 269.3 \text{ kip}$$

Beam Flange Force at FLB Limit State

$$P_{f,FLB} := 702.4 \text{ kip}$$

Connection Force Added with eccentric continuity plates

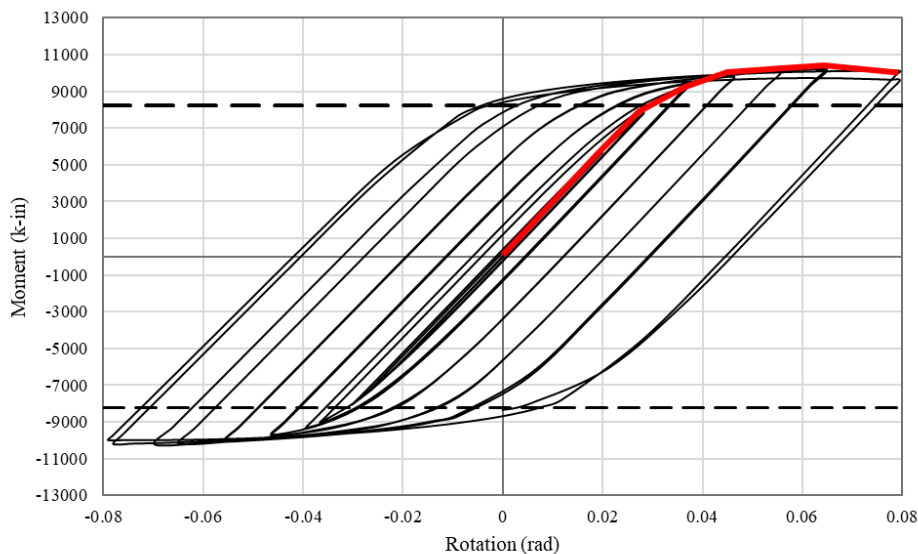
$$\frac{P_{f,FLB} - \phi R_{n,FLB}}{P_{f,FLB,max} - \phi R_{n,FLB}} = 74\%$$

See Figure 21 and Figure 22 to see these percentages plotted

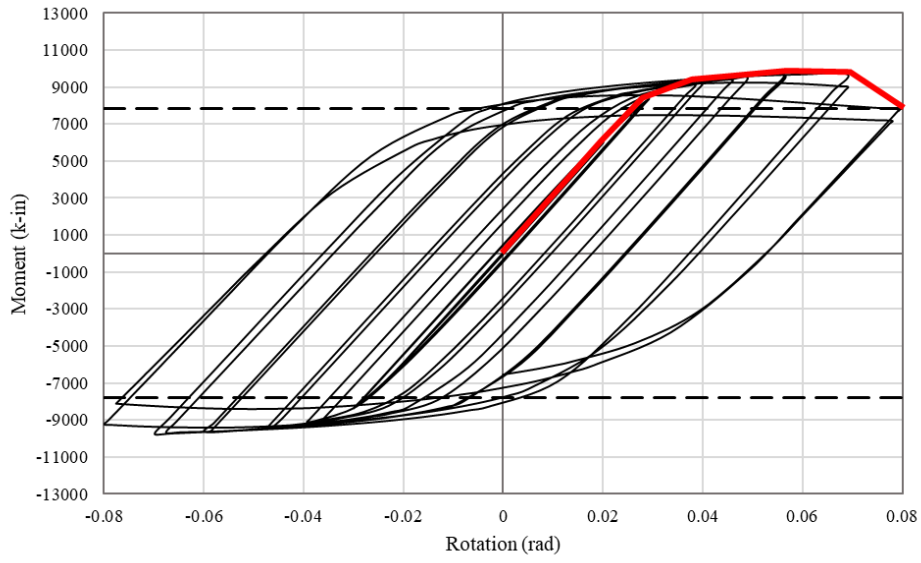
A3. Selected Hysteresis Graphs

Figure 23 shows selected hysteresis graphs for the W14x132 columns at various eccentricities. They are shown to demonstrate the effects of eccentricity on rotational capacity of the column. The dashed lines represent $0.8M_p$ for the configuration and the red line represents the backbone curve for the configurations. From these figures, it becomes apparent that significant effects on rotation capacity begin to occur as eccentricity increases past 4 in.

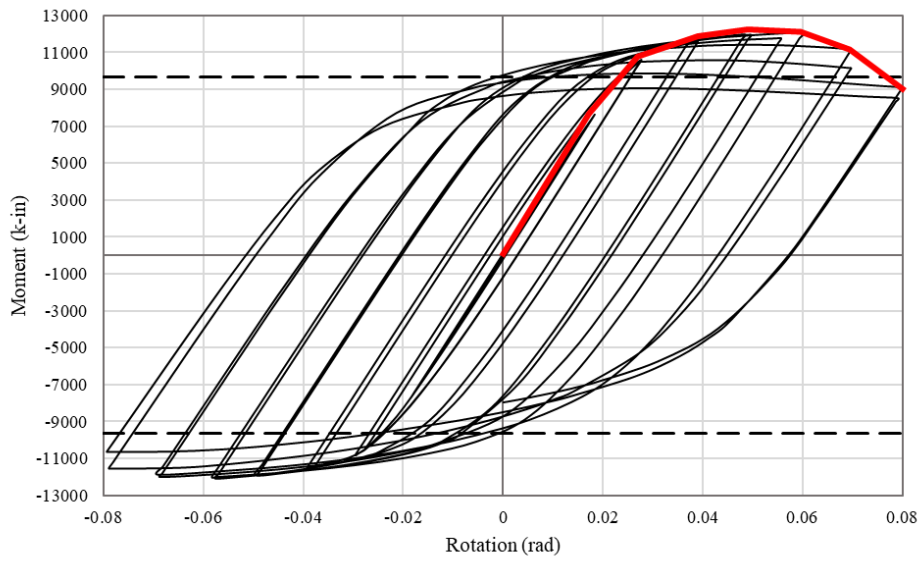
From the hysteresis graphs, it is apparent that increasing the eccentricity decreases the rotational capacity of the connection, regardless of the limit state in question. Figure 23 shows that by 5.83 in. eccentricity, the connection is reaching M_p at 0.04 rad., compared to the inline connection that reaches M_p at 0.07 rad. This observed rotational capacity aligns well with the current FLB limit state eccentricity allowance in the provisions [4].



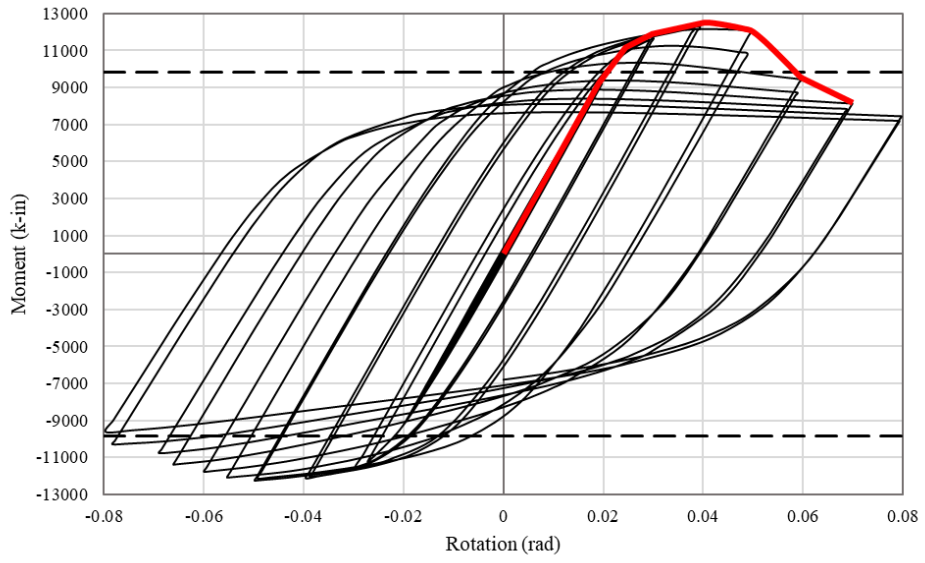
(a)



(b)



(c)



(d)

Figure 23. Hysteresis graphs for W14x132 configurations for various eccentricities (a) 0 in. (b) 1.645 in. (c) 4.125in. (d) 5.83 in.

A4. Proposed Design Approach

To show how Equation 4 is intended to be used, a proposed design approach is shown below. The equation is intended to be a simple check to determine whether an eccentrically stiffened column flange is adequate without further stiffening needed. The connection is shown to be adequate concerning FLB, but not adequate if concerned about FLY.

| | | | |
|---|--|----------------|----------------------------------|
| Column: W24x176 | | | |
| Beam 1: W16x100 | | | |
| Beam 2: W18x106 | | | |
| $M_{pc} := 23653 \cdot \text{kip} \cdot \text{in}$ | $\Sigma M_{pc} := 2 \cdot M_{pc} = 47306 \text{ kip} \cdot \text{in}$ | | |
| $M_{pb1} := 12524 \cdot \text{kip} \cdot \text{in}$ | | | |
| $M_{pb2} := 12903 \cdot \text{kip} \cdot \text{in}$ | $\Sigma M_{pb} := M_{pb1} + M_{pb2} = 25427 \text{ kip} \cdot \text{in}$ | | |
| $\frac{\Sigma M_{pc}}{\Sigma M_{pb}} = 1.86$ | $1.86 \geq 1.0$ | \therefore | Connection satisfies SC/WB check |
| $F_y := 50 \cdot \text{ksi}$ | $t_{cf} := 1.34 \cdot \text{in}$ | $\phi := 0.90$ | |
| $\phi R_{n,FLB} := \phi \cdot 6.25 \cdot F_y \cdot t_{cf}^2 = 505 \text{ kip}$ | | | |
| $d_{b1} := 17.0 \cdot \text{in}$ | $d_{b2} := 18.7 \cdot \text{in}$ | | |
| $t_{b1f} := 0.985 \cdot \text{in}$ | $t_{b2f} := 0.94 \cdot \text{in}$ | | |
| $R_{ub1} := \frac{0.85 \cdot M_{pb1}}{d_{b1} - t_{b1f}} = 664.7 \text{ kip}$ | $R_{ub2} := \frac{0.85 \cdot M_{pb2}}{d_{b2} - t_{b2f}} = 617.5 \text{ kip}$ | | |
| $R_{ust} := \max(R_{ub1}, R_{ub2}) - \phi R_{n,FLB} = 159.7 \text{ kip}$ | | | |
| use 0.75 in. thick, full width, full depth continuity plates | | | |
| $A_{st} := 9.11 \cdot \text{in}^2$ | $F_y := 36 \cdot \text{ksi}$ | | |
| $\phi R_{nst} := \phi \cdot F_y \cdot A_{st} = 295.2 \text{ kip}$ | $295.2 \text{ kip} \geq 159.7 \text{ kip}$ | \therefore | adequate |
| However, these beams are not the same depth, thus there is an eccentricity. | | | |
| $e := (d_{b2} - t_{b2f}) - (d_{b1} - t_{b1f}) = 1.745 \text{ in}$ | | | |
| $\phi R_{necc} := \phi R_{n,FLB} + R_{ust} \cdot (-0.039 (e^2 + e - 25)) = 630.9 \text{ kip}$ | | | |
| $630.9 \text{ kip} \geq 617.5 \text{ kip} \checkmark$ | | | |